Comprehensive Real-Time Simulation of the Smart Grid

Feng Guo, *Student Member, IEEE*, Luis Herrera, *Student Member, IEEE*, Robert Murawski, *Member, IEEE*, Ernesto Inoa, *Student Member, IEEE*, Chih-Lun Wang, Philippe Beauchamp, Eylem Ekici, *Senior Member, IEEE*, and Jin Wang, *Member, IEEE*

***Abstract*—This paper presents a real-time simulation platform for smart grid applications. The developed platform is capable of simulating complex smart grid models with large numbers of high-speed switching devices at real time. Furthermore, an integrated approach is adopted to combine real-time simulations of communication systems and electric power systems together, which provides an effective approach to examine communication and distributed control related issues in smart grids. With the flexibility in representing a wide range of communication network configurations, the developed platform can also be used to evaluate reconfiguration strategies of communication networks in smart grids. A case study is demonstrated based on this platform. Simulation results validate the capability of the platform and also show the importance of the proposed comprehensive approach for the study of smart grids.**

***Index Terms*—Communication network, real-time simulation, smart grid.**

I. Introduction

THE TERM "smart grid" encompasses up-to-date technologies in areas such as power electronics, communication, and renewable energy resources in order to establish a more secure, reliable, economic, and eco-friendly electric power system [1], [2]. A smart grid usually contains different kinds of renewable energy resources, such as photovoltaic (PV), wind turbine, battery storage system, etc., and a large number of power electronics interface circuits. Thus, experimental studies of large-scale smart grids are usually not economically feasible. As an evidence, even for microgrid, where the number of distributed energy sources and intelligent loads is quite limited, there are only a handful test platforms around the world [3], [4]. Therefore, simulation becomes a powerful and convenient tool in this research area.

Manuscript received May 24, 2011; revised December 3, 2011; accepted December 12, 2011. Date of publication January 16, 2013; date of current version March 15, 2013. Paper 2011-IPCC-299.R1, presented at the 2011 IEEE Energy Conversion Congress and Exposition, Phoenix, AZ, USA, September 17–22, and approved for publication in the IEEE TRANSACTIONS ON INDUSTRY APPLICATIONS by the Industrial Power Converter Committee of the IEEE Industry Applications Society. This work was supported by the U.S. Department of Energy under Project DE-OE-0000402.

F. Guo, L. Herrera, R. Murawski, E. Inoa, E. Ekici, and J. Wang are with The Ohio State University, Columbus, OH 43210 USA (e-mail: guof@ece.osu.edu; herrera.46@buckeyemail.osu.edu; murawski.8@osu.edu; einoa@ieee.org; ekici@ece.osu.edu; wang@ece.osu.edu).

C.-L. Wang is with Ford Motor Company, Dearborn, MI 48120, USA (e-mail: wang.1376@osu.edu).

P. Beauchamp is with Opal-RT Technologies, Montreal, QC H3K 1G6, Canada (e-mail: philippe.beauchamp@opal-rt.com).

Color versions of one or more of the figures in this paper are available online at http://ieeexplore.ieee.org.

Digital Object Identifier 10.1109/TIA.2013.2240642

The integrated power electronics devices in the smart grid introduce two great challenges to the simulation: high-frequency pulse width modulation signals and large numbers of switching devices. As a result, traditional offline simulators are time consuming for long period simulations and not suitable to study slow phenomena [5]. Moreover, this kind of simulation usually lacks the hardware interface with real devices; thus, it cannot be used at all the development stages of the smart grid, such as prototyping and testing.

As early as 20 years ago, manufactures of large thyristor-based high-voltage direct current and Flexible AC Transmission Systems devices have used the digital real-time simulator and hardware-in-the-loop (HIL) methods to solve the aforementioned problems for power system with relatively slow frequency and small numbers of switches [6]. After two decades of developments, the digital real-time simulator can run a large and complex model at the physical time; thus, it is suitable to simulate a long-time frame process. In addition, with the support of the real-time simulator, power-in-the-loop can be utilized for testing of high-power devices that are connected to complex systems.

The requirement for real-time simulation of high-frequency switching devices was brought forward by the manufacturers of fast power electronics devices such as Mitsubishi more than five years ago [7]. The real-time simulator in [7] can run the simulation with a time step of 10 μs for one three-phase inverter. In [8], a field-programmable gate array (FPGA)-based real-time simulator can reach a time step of 500 ns for a diode-clamped three-level voltage source converter. However, for a system with large numbers of switching devices, it becomes difficult to achieve such small time step, and specific consideration is still needed. A microgrid model with two renewable energy sources and two inverters in [9] is only able to run with a switching frequency of 1 kHz at real time. Therefore, sufficient research and new methods are still needed to speed up the adoption of real-time simulation on smart grid.

On the other hand, the communication network is essential to effectively incorporate many of desired features of the smart grid such as distributed automated system, distributed energy resource protection, islanding, and display of network state and performance [1]. Thus, another challenge in smart grid study is to integrate different kinds of communication networks and simulate their influence to electric power systems at real time. In [10], Nutaro *et al.* developed an offline software simulation of a 17 bus power network with communication between loads and generators, investigating the effects of factors such as

bandwidth and latency. RTDS-based systems for testing protective relays in power networks have been discussed in [11] and [12], but with a separate study on communication networks. In [13], a real-time HIL model of a power network was implemented along with a physical network of two nodes: the real-time simulation and a physical remote control center. The control center served as a means of monitoring and controlling the overall system, and testing cyber vulnerabilities of it. In sum, the importance of emulating communication network in smart grids becomes apparent. An effective modeling of communication between control centers along with present real-time simulation of power networks could show more realistic results and bring great benefits to related studies in smart grids.

This paper presents a comprehensive platform to overcome current challenges in smart grid related real-time simulation. In Section II, theoretical analysis showcases the reason of detailed modeling communication network in smart grid related study. Section III introduces the platform, and the solutions to the challenges. Section IV describes a case study, and Section V illustrates the simulation results. Finally, in Section VI, summary and conclusion are presented.

II. Communication Network Modeling and Simulation

Communication networks are expected to be integrated components of smart grid systems. The coexistence of communication and power networks and their joint operation necessitate accurate modeling of communication events. While at the first glance, it is tempting to model the communication network as a black box that introduces delays between its input and output, the complex interactions among network components and between data sources and the network make it less tractable. To illustrate this, consider a case that requires dynamic reconfiguration of the communication network based on changing operating conditions of the power network. Assume that the operation of a microgrid is controlled by a Microgrid Control Center (MCC). To this end, the controller relies on data periodically collected from power sources and loads. Since most data sources are distributed over large geographic areas, at this point, it is assumed that the said data is delivered to a centralized access point (AP) via wireless links using Carrier Sense Multiple Access/Collision Avoidance (CSMA/CA) principles, which is the most widely used channel access scheme in today's wireless devices including IEEE 802.11 compliant ones. The information is then relayed to controllers via a wired connection. The portion of interest of the communication network is shown in Fig. 1, which consists of 20 reporting nodes, one AP, and the controller. Consider two operation modes for the network: ***A. Regular Operation Mode***: Data sources report their readings at a rate of λ_{A} packets/s/source, which are collected at AP and delivered to the controller in T_{A} s; ***B. Exception Operation Mode***: Events in the power network causes the reporting rate to rise to λ_{B} packets/s/source. Messages must be reported to the controller in T_{B} s.

Consider the transition from the Regular to the Exception Operation Mode and its effects on the communication network. Assume that this transition results in the changes to the reporting rate only such that $\lambda_{\mathrm{B}} > \lambda_{\mathrm{A}}$, while the reporting delay remains constant, i.e., $T_{\mathrm{B}} = T_{\mathrm{A}}$. As a general principle, the latency of message delivery in random access networks increases exponentially as the load offered to a wireless network operating under CSMA/CA rules increases. The goal is to control the topology and channel access rules while retaining the CSMA/CA principles to ensure stability of the power network. Assume that there is a function F based on existing non-saturation CSMA/CA performance models such as [14] that can estimate the average service rate μ_0 based on the number of competing nodes N and the per node packet arrival rate λ as $\mu_0 = F(N, \lambda)$. Then, the average packet delay D_0 including the queuing time can be estimated using the M/M/1 queuing model as $D_0 = 1/(\mu_0 - \lambda)$ s. Now, consider the option of grouping the nodes into K groups such that, at any given time, only N/K of the nodes contend for channel access while others wait for their turn to contend. This can be achieved by dividing the time into slots of length t. Each group can access the channel every K time slots, where t is long enough to serve several packets. In Fig. 2, two cases are identified where $K = 1$ (group marked with dotted lines) and $K = 4$ (groups marked with red dashed lines). Using the model represented by the function F, the service rate of single region can be estimated as $\mu_{\mathrm{k}} = F(N/K, \lambda)$. Then, the average packet delay D_{k} for a K group arrangement can be estimated as $D_{\mathrm{k}} = t((K-1)/2 + \lfloor 1/(t(\mu_{\mathrm{s}} - \lambda)) \rfloor K + 1)$, to account for the delay experienced during inactive slots and while contending for the channel.

The average packet delay is shown as a function of per node arrival rate in Fig. 2 for $t = 35$ ms for $K = 1$ and $K = 4$.

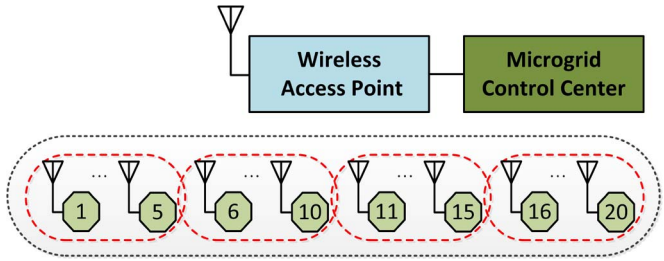

Fig. 1. Communication network.

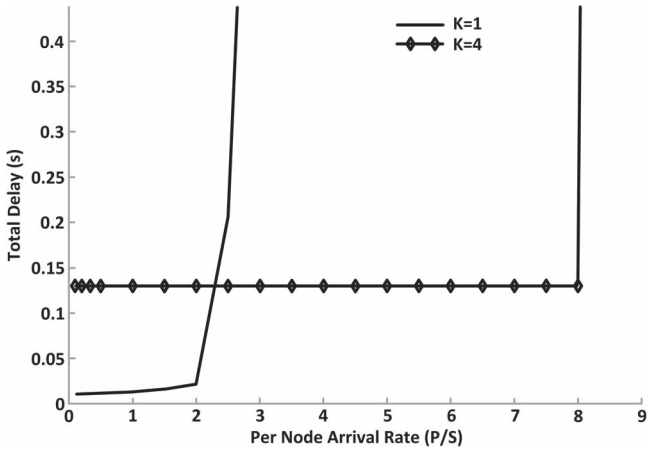

Fig. 2. Average latency versus per node arrival rate.

$K = 1$ provides significantly lower latency to packets when the reporting rate is below $\lambda = 2.5$ packets/node/s. When the arrival rate increases further, the delay increases exponentially. The delay of any node for the $K = 4$ case is dominated by the waiting time between active time slots. Grouping the nodes into smaller contention groups significantly reduces the random access delay. Hence, $K = 4$ is more suitable for higher arrival rates: For $\lambda > 2.5$ packets/node/s, the average delay is significantly lower for $K = 4$ than for $K = 1$. Inevitably, the exponential growth of latency occurs as the arrival rate increases. However, this occurs for $\lambda > 8$ packets/node/s, which is significantly higher than the threshold for $K = 1$. For $T_{\mathrm{A}} = T_{\mathrm{B}} = 150$ ms and $\lambda_{\mathrm{A}} < 2.5$ packets/node/s in the regular operation mode, $K = 1$ is sufficient. If switching to exception operation mode results in an arrival rate larger than 2.5 packets/node/s, then the communication network should be reorganized with $K = 4$. It should be noted that $K = 1$ and $K = 4$ are not the only two options. Different reorganizations with different parameters are also possible. Moreover, it is also possible to organize the network into a hierarchy deeper than two levels (i.e., including intermediate levels between reporting nodes and the AP).

As highlighted in the preceding example, the highly nonlinear relationship between the source rates and the resulting delays across the network is a significant hurdle to overcome. In most analytical models that relate arrival rates to network latencies, the relationship is established among the first-order statistics of the input and output random variables. Except in simplest of cases, it is not possible to derive tight bounds on delays, or other relevant metrics such as loss rates. Moreover, most analytical models' accuracy suffers greatly as the network size grows from single hop settings to relay networks. On the other hand, there are a number of simulation platforms that replicate the behavior of communication networks relatively accurately. While these simulation tools cannot generate analytical results, their estimation of delay and loss parameters vis-a-vis actual operation of the communication network is very accurate. Reserving the use of stochastic model for future studies of network design, this paper concentrates on developing a simulation platform that mimics both the power network as well as the communication network operation accurately. With the ability to simulate a wide range of communication network configurations, the developed platform can also be used to evaluate various designs and reconfiguration strategies for an actual smart grid.

III. Real-Time Simulation Platform

The real-time simulation platform presented in this paper (see Fig. 3) is based on PC technology running a Linux operating system and offers an underlying test bed for the study on smart grid. It consists of four real-time simulators with a total of eight CPUs, 48 cores, five FPGA chips, and more than 500 analog and digital inputs/outputs [15]. Dolphin [16] PCI boards are used to provide an extremely high-speed and low-latency real-time communication link between simulators.

1) Electric Power System Simulation: With the technology of switch event interpolation [5], State Space Nodal (SSN) solver [17], and parallel computation, the system provides an effective way to simulate a system with large numbers of high-frequency switching devices.

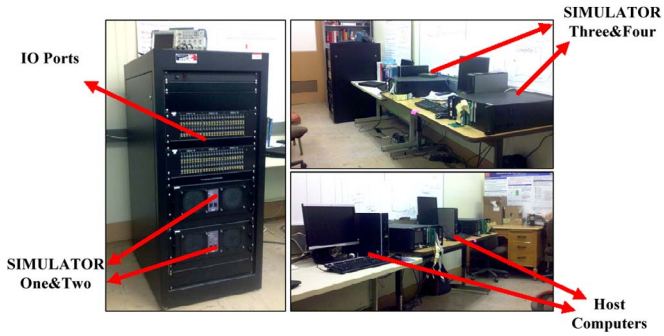

Fig. 3. Real-time simulation platform.

The challenge of simulating models with high-speed switching devices is the small step size required to achieve adequate simulation accuracy. Selecting too large of a step size will produce an erroneous simulation output and selecting too small of a step size will not be able to meet the real-time constraint. The solution to this problem is the switch event interpolation technology, which combines software solving algorithms with high-end hardware technology. The RT-EVENTS software library [15] in combination with FPGA is used to handle discrete events that occur inside one model calculation step, which allows the model to run with a larger step size without sacrificing simulation accuracy. The switching devices can also be modeled directly inside the FPGA in order to obtain higher switching frequencies for specific applications.

The limitation of the number of switches that can be used in a real-time model is caused by the $\mathrm{O}(2^{\mathrm{N}})$ computational complexity. It will increase a great number of inverse matrices to be computed for each additional switch when the total number of switches becomes large. This problem was addressed by the SSN solver, which uses a combination of the nodal approach and the state space solver approach. SSN solver decouples the whole system state-space matrix into small groups of matrices, thus reducing the overall computational complexity. Benchmarks have shown that it is possible to run simulations with more than 100 switches in a single subsystem.

Furthermore, relying on the parallel computation capability, this system is able to run a complex power system model with a maximum of 48 subsystems, which can further increase the switching frequency and number of switching devices in the model. In this approach, the smart grid model will be intentionally divided into small subsystems. Each subsystem can be either a renewable energy resource unit, such as a PV model, wind turbine model, or a controller unit. These will be distributed into cores in different simulators, which will be executed and synchronized with high precision.

In general, with the help of the presented real-time simulation system, a switching frequency up to 10 kHz can be achieved, and a large number of switches can be included in one model. Moreover, the system allows multiple users to be connected to the real-time simulator concurrently to perform collaborative simulation, for which distributed control and HIL operation can be easily realized.

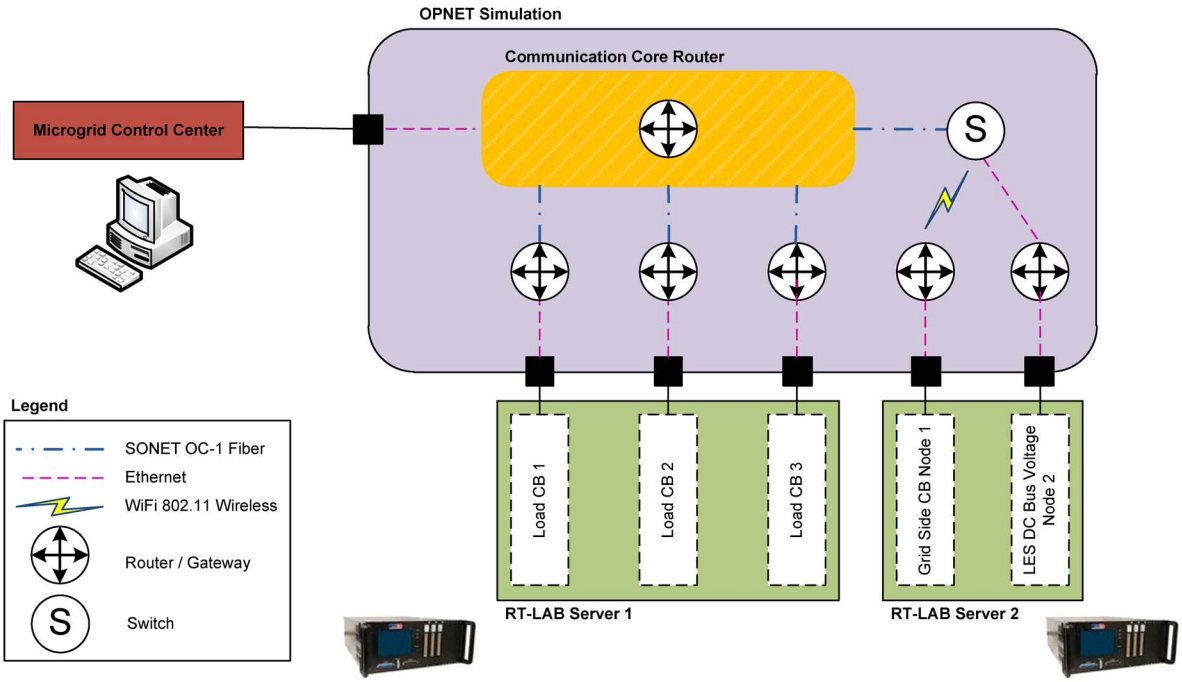

Fig. 4. SITL model of the communication network.

2) Communication System Simulation: When combined with a discrete network simulator, the real-time simulation system can provide advantages to simulating communication network and distributed control in the smart grid in a cost effective manner. Such studies would allow identification of the influence of key communication factors to the smart grid, such as protocols, latency and bandwidth requirements, cyber security, and data management [2].

OPNET [18] is a commercially well-developed network simulator that has been used extensively in research. A system-in-the-loop (SITL) package is available for use with OPNET that bridges the OPNET network simulation with the hardware simulation. It has the ability to accept real-time network traffic and simulate either a wired or wireless network. OPNET allows significant flexibility in terms of network development; this, combined with the integrated support of many well-known communication protocols, makes OPNET an excellent option for implementation of the proposed communication network.

Fig. 4 shows an example of communication network model using SITL gateways to link with power network model. Each key power network device, such as sensors, breakers, control center, etc., will be assigned its own IP subnet and, therefore, will require the simulated network to route packets between them. Within the OPNET environment, IP traffic is accepted at different SITL gateways by filtering traffic by the source address. In Fig. 4, a total of six SITL gateways are utilized within OPNET. Five gateways are connected to the simulated power network interfaces. The sixth gateway connects to the MCC which gathers information and distributes control messages to the power network as required. Each device has a router associated with it which routes the IP layer traffic to its intended destination based on pre-defined static routing tables. By placing the SITL gateways, simulated routing, and switching hardware within OPNET, different distances between power network devices and the delays and bit error rates associated with transmitting packets can be simulated. In addition, different virtual network types can be chosen between gateways, such as Ethernet, wireless, and fiber optic, depending on the transmission distance and data type in a real power network. OPNET SITL also allows the transmission of individual packets from the input ports to the output ports of the simulated network by following the exact steps of buffering, protocol processing, transmission, and reception.

When combining the power system (continuous time system) and communication system (discrete time system) together, the proposed platform runs both systems at real time and simultaneously solves two distinct models in parallel. This has an advantage in terms of synchronization of the systems since both power and communication network models are running at the same rate as a "wall clock." The simulation setup is shown in Fig. 5. The mathematical model of the power network is first built in Matlab/Simulink environment, then converted to real-time model, and finally solved by the Linux based real-time simulators; whereas the communication network is modeled using the discrete network simulator OPNET running on another desktop computer. A second desktop computer is utilized as the MCC server, and the information sent from the OPNET network is processed in it.

Meanwhile, the power system model has the capability of information exchange through an external Ethernet connection, so power and communication systems can exchange information through physical Ethernet links. An external C code is developed for Linux systems which develops the necessary layers for real-time information exchange using TCP/IP or UDP/IP protocols. Therefore, the corresponding data in power system model is sent to the external computer running OPNET through physical Ethernet links. Within OPNET, the traffic is filtered from the interface by the source address and thus creating

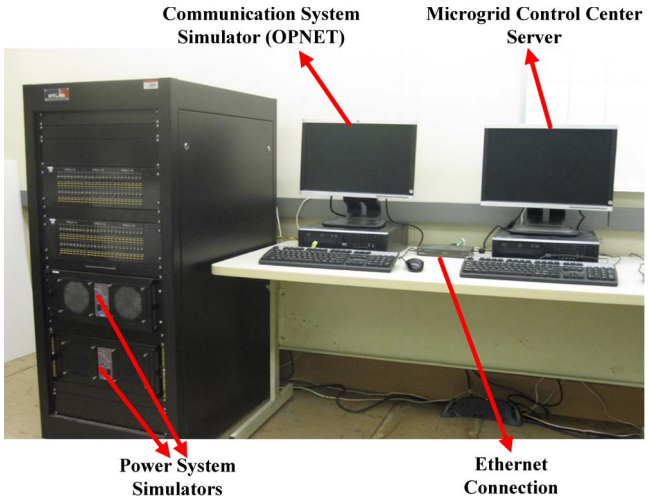

Fig. 5. Combined simulation platform of power system and communication system.

different nodes for building an accurate communication network. Information is then processed in real time within OPNET and sent to the MCC server through another Ethernet link. After necessary calculation, the MCC sends back the control command to OPNET, which then distributes the information to the corresponding destinations within the power system model.

In conclusion, with the cooperation of advanced software and hardware, and the combination of power network simulator and communication network simulator, the platform presented in this paper is able to provide a comprehensive approach for smart grid-related study.

IV. Case Study

A. Model Description

In this section, the smart grid in a small community is modeled with the developed real-time simulation system. The model includes a Local Energy Storage (LES) device, a PV-based generator, a wind turbine, as well as the communication network described in Fig. 4. The system is shown in Fig. 6.

Each unit in the smart grid is modeled with detailed characteristics. The LES is modeled as recycled electric car batteries. The impedance and output voltage of LES are not only determined by the State of Charge (SOC), but also the temperature inside the LES [19]–[22]. The PV is built with the mathematical model described in [23]. The output voltage and power of this unit are related to the irradiation and environment temperature. The wind turbine is modeled as a doubly fed induction generator (DFIG) with back-to-back inverters. The noncritical load is modeled as a nonlinear load powered through power electronics circuits, while the critical load is modeled as a three-phase resistive load. Additionally, all circuit breakers in the system are modeled as solid state circuit breakers. In total, there are nearly 100 switches in the model operating at a switching frequency of 10 kHz. Furthermore, because the switching actions will influence the whole system characteristics, in order to simulate the system in a more precise way, the switching frequency is kept at 10 kHz in both grid-connected mode and islanding mode. This detailed modeling also enables further HIL-based study.

The MCC within the smart grid is able to serve the following purposes: changing the settings of protection devices based on either grid-connected or islanding mode, monitoring values within the smart grid, and sending signals to reconfigure the smart grid depending on its current configuration [24]. In the model, all circuit breakers are equipped with transmitter and receiver units, which are able to send its status to the MCC as well as acquire control signals. In order to achieve a low latency, the circuit breakers of noncritical loads communicate with the core router at the MCC through simulated fiber optic cabling using the Synchronous Optical Network standard at OC-1 speed (51.8 Mbps). The main circuit breaker at the point of common coupling (PCC) connects to a separate router via WiFi 802.11 wireless communication, since it is usually located far away from the MCC. While the LES dc bus voltage node connects to the separate router via Ethernet. As stated in Section III, the communication network is emulated by OPNET while the MCC is implemented in an external computer.

The simulation parameters are shown in Table I.

B. Control Strategy

The aim of the controller design is to make sure the system works properly in both grid-connected mode and islanding mode. More importantly, the controller should avoid large voltage and current spikes during the transition from grid-connected mode to islanding mode.

1) Grid-Connected Mode: In grid-connected mode, a multi-loop controller is used for all the three grid tied inverters. The control objective of the inverters is to keep the dc-link voltage constant. The outer loop of the controller consists of a voltage loop with dc-link voltage as feedback. The inner loop is a grid current control loop, with the active current reference generated by the outer voltage loop and reactive current reference set to 0, as shown in Fig. 7.

Referring to the circuit diagram in Fig. 6(b), the simplified current open-loop transfer function in dq-rotating reference frame is

$$\frac{I_d}{V_{dl}^*} = \frac{1}{L_f s + R_f}. \tag{1}$$

The response of the inner current loop should be much faster than the outer voltage loop, hence a proportional–integral (PI) controller is used to achieve a good system performance. The design of the voltage control loop is based on the assumption that the inner current loop is ideal. The open-loop transfer function is

$$\frac{V_{\rm dc}}{I_d^*} = \frac{1}{Cs}. \tag{2}$$

Again, a PI controller is applied to get the required system response characteristics.

The control of the rotor side inverter of the DFIG follows the strategy in [25]. A decoupled control between the electric torque and rotor excitation current is achieved by a rotating

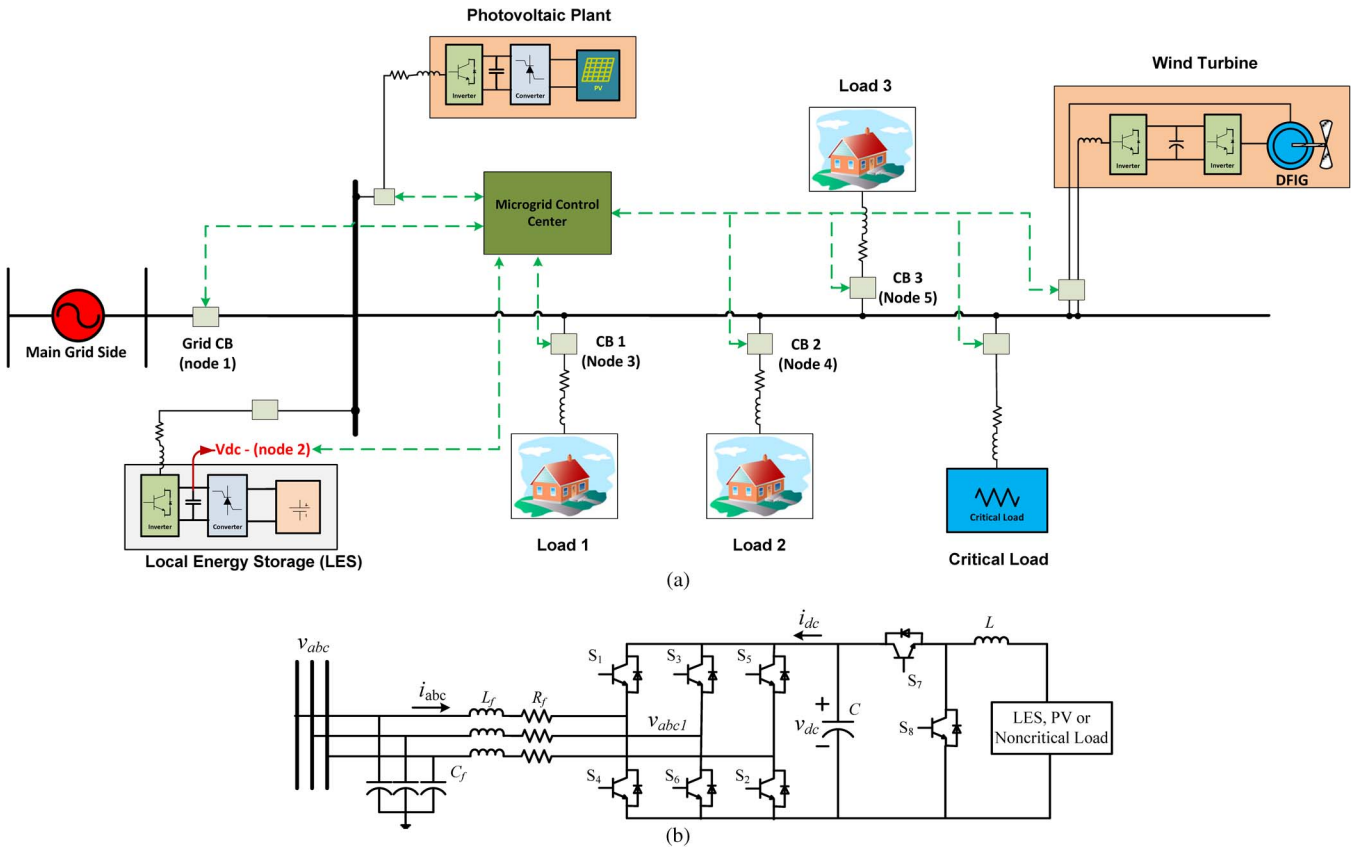

Fig. 6. Illustration of the case study: a small community microgrid. (a) System diagram; (b) detailed circuit topology.

TABLE I
SIMULATION PARAMETERS

System Frequency f	60 Hz
Switching Frequency f_{sw}	10 kHz
Dc Bus Voltage V_{dc}	800 V
Capacitor C	4.4 mF
Ac Bus Voltage V_{bus}	240 $V_{L\text{-}g}$
Inductor L_f	0.76 mH
Resistor R_f	1 mΩ
Capacitor C_f	8.3 μF
PV Power P_{PV}	5.3 kW
Wind Turbine Power P_{Wind}	10 kW
Critical Load Power Consumption $P_{critial}$	10 kW
Noncritical Load Power Consumption $P_{noncritial}$	15 kW

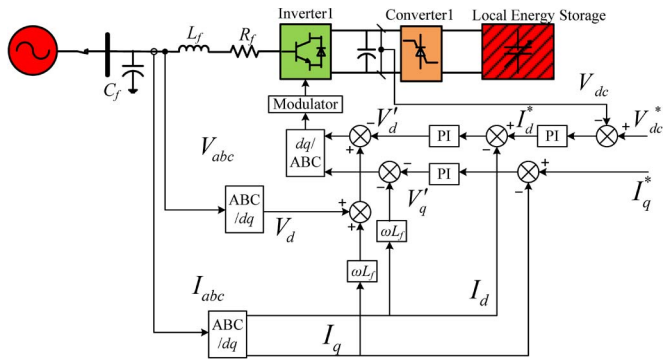

Fig. 7. Control strategy of the LES-connected inverter during grid-connected mode.

dq axis frame with the d-axis oriented along the stator flux vector position.

Considering the converters, the LES-connected converter and noncritical-load-connected converter are working in current control mode, while the PV-connected converter is working with Maximum Power Point Tracking (MPPT) strategy.

2) Islanding Mode: In islanding mode, the inverters and converters connected to PV and DFIG are still controlled current sources as in the grid-connected mode. However, the LES-connected inverter, because of the loss of the grid, is controlled to be a voltage source to function as the swing bus of the system. The same multi-loop control structure is utilized for the LES inverter, but with the ac bus voltage as feedback in the outer voltage loop, as illustrated in Fig. 8. The inner loop is the same current control loop as in grid-connected mode.

The current open-loop transfer function in islanding mode is slight different from grid-connected mode, which becomes

$$\frac{I_d}{V_{dl}^*} = \frac{C_f s}{L_f C_f s^2 + R_f C_f s + 1}. \tag{3}$$

A PI controller is implemented for the current control. At the same time, the open-loop transfer function for the outer voltage loop becomes

$$\frac{V_d}{I_d^*} = \frac{K_{cp} s + K_{ci}}{L_f C_f s^3 + (R_f C_f + K_{cp} C_f) s^2 + (K_{ci} C_f + 1) s} \tag{4}$$

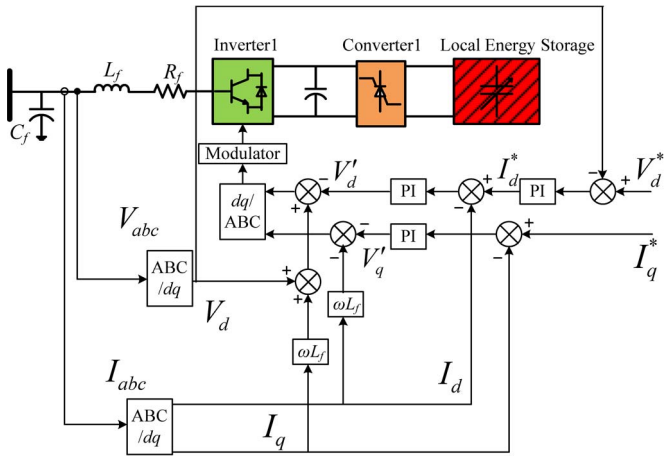

Fig. 8. Control strategy of the LES-connected inverter during islanding mode.

where K_{cp} and K_{ci} are the proportional gain and integral gain of the current PI controller. A PI controller is applied as well to reach the voltage control requirement.

As mentioned above, in islanding mode, the LES-connected inverter is used to control the ac bus voltage. Therefore, the control purpose of the LES-connected dc/dc converter is changed to control the dc-link voltage. Considering that the output current of the LES should also be tightly controlled, a multi-loop control structure with outer voltage loop and inner current loop is designed for this converter. The outer voltage control loop uses the dc-link voltage as feedback, which will generate a reference current value for the inner control loop.

As shown above, the only noticeable difference between control strategies in grid-connected and islanding mode is that the voltage reference of LES-connected inverter is changed from the dc bus voltage to ac bus voltage. Therefore, there is no sudden change on the local controllers, and a seamless transition from grid-connected mode to islanding mode can be achieved.

The whole system operation indeed requires a high level of coordination, which is realized with the MCC. When the maximum power from the PV and wind turbine could be fully absorbed by the load and the battery, the PV and wind turbine will be commended to operate in MPPT mode. If the LES battery reaches its upper limit of SOC and the power supply from renewable energy sources is higher than the load demand, which usually is rare, the PV and wind turbine will be commended to reduce power output. During the transient of dynamic islanding, load shedding and reconnection will also be performed if the MCC predicts that the power generation is less than the demand.

V. Simulation Results

A. Results Without Considering the Latency of the Communication Network

Real-time simulation was performed for the case where the system transfers from grid-connected mode to islanding mode. First, only the power network and associated control strategies were simulated and evaluated. In the simulation, a three-phase short circuit occurs on the grid side. A protection scheme to detect loss of main, which is developed based on the control discussed in [26], detects the failure and opens the main circuit breaker at the PCC. It is assumed that during islanding mode, the LES, PV, and wind turbine can provide enough power for both critical and noncritical loads.

Since the simulation is running at real time, the simulation results could be observed via oscilloscope. Oscillograms of simulation results of the dc bus voltage within LES inverter system, ac bus voltage, and LES output ac current are shown in Fig. 9(a), and ac currents from grid side, PV, wind turbine, critical load, and noncritical load are shown in Fig. 9(b). The results illustrate that when the system changes from grid-connected mode to islanding mode, the dc bus voltage, ac bus voltage, and load currents remain constant. Moreover, the voltage and current spike during this transition are within two times of their normal values, which is not significant. Therefore, the proposed control strategy is effective, and the real-time simulation platform successfully handles the complex smart grid model with a large number of switching devices that are operating at high frequency.

B. Comprehensive Results With Communication Latency

Real-time simulation was then performed to test the influence of the communication on the power network. In this case, both power network and communication network were simulated and evaluated. It is assumed that during islanding mode, the LES, PV, and wind turbine cannot provide enough power for all loads; consequently, load shedding is necessary to maintain the system stable. In islanding mode, the LES can provide a maximum power of 8.3 kW, the PV 5.3 kW, and the wind turbine 10 kW. On the load side, the power consumption of each noncritical load and critical load is 5 kW and 10 kW, respectively. The dc bus threshold voltage is 730 V.

Considering the communication effect, during a fault on the grid side, the main circuit breaker at the PCC will open and send a signal to the MCC which initiates islanding mode and disconnects the three noncritical loads simultaneously. Furthermore, the LES dc bus voltage is monitored by the MCC and gives a status of the power capability of the smart grid. The MCC will start reconnecting noncritical loads one at a time every 0.1 s. If the monitored LES dc bus voltage is constant, the smart grid is able to sustain itself. However, if the voltage begins to decrease, the MCC will disconnect the last load added to the system, and the load shedding process stops. The effects of latency, bandwidth, and packet losses will introduce behaviors in the overall network which can be studied and compared.

Fig. 10 shows the real-time simulation results without the communication effect, Fig. 10(a), and with the communication effect, Fig. 10(b). The local dc bus voltage value and the dc bus value detected by the MCC were monitored with the same digital oscilloscope; they are both shown in the figures to identify the total communication delay. In the first case, the communication between nodes is ideal and instantaneous data transfer. All the noncritical loads were cut off at the beginning of the dynamic islanding at t1. Then, one by one, each noncritical load is reconnected after every 0.1 s. At the

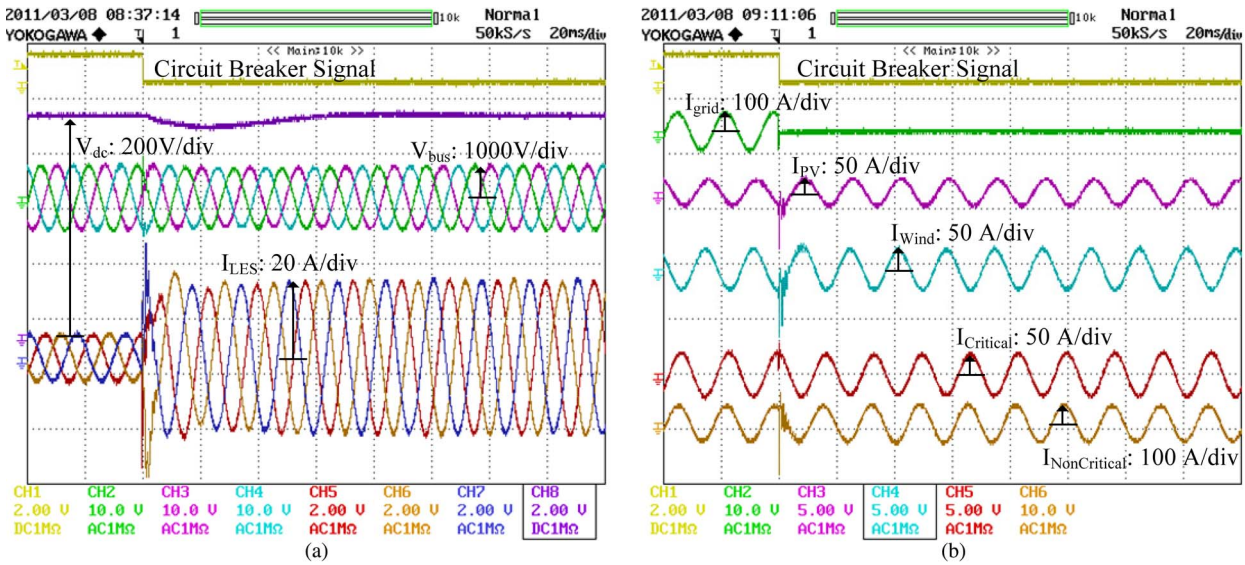

Fig. 9. Simulation results for intentional islanding. (a) dc bus voltage within LES subsystem, ac bus voltage, and LES output ac current; (b) ac currents from grid side, PV, wind turbine, critical load, and noncritical load.

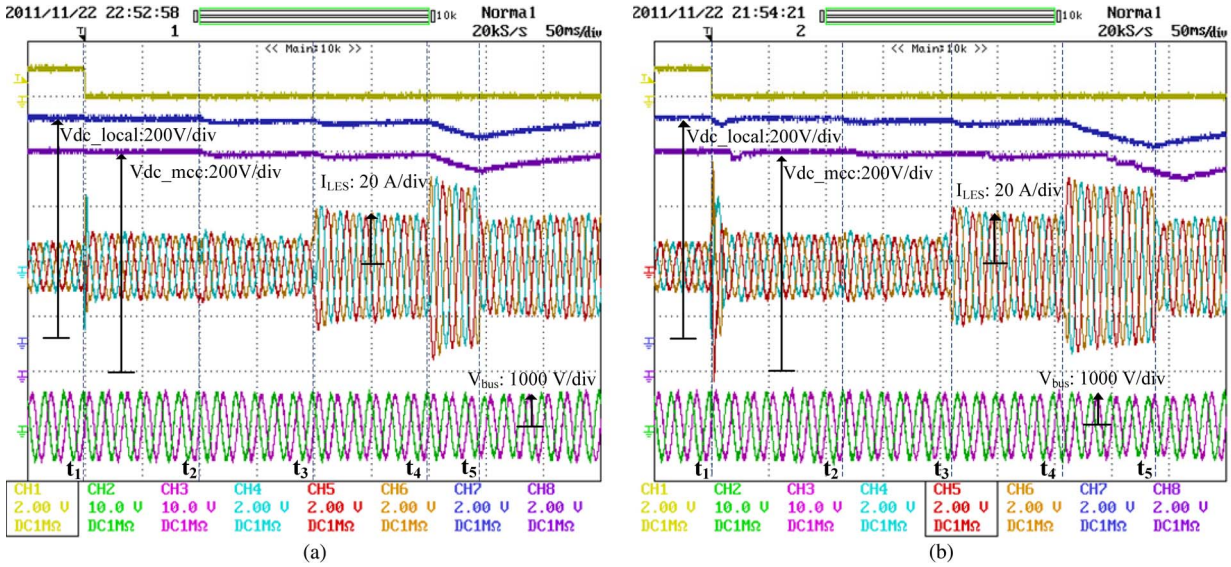

Fig. 10. Simulation results for load shedding. (a) Ideal communication (no delay); (b) communication with delay.

same time, a sensing unit measures the LES dc bus voltage and sends it to the MCC. When the last noncritical load was reconnected at t4, the dc bus voltage of LES starts to drop due to power imbalance. When the dc bus voltage drops to the threshold voltage at t5, CB3 is reopened by the MCC, and the dc bus voltage of LES returns to its normal value.

In the second case, the communication network is not ideal. It is assumed the MCC sends out data every 10 ms. Moreover, because of the distances between different nodes and the MCC, different latencies during the data transmission paths are produced. Compared to the first case, the influence of the communication network can be found as follows: 1) Since the MCC sends out data every 10 ms, the noncritical loads cannot be disconnected from the grid at the same time the main circuit breaker opens, which results in a larger disturbance during the transition; 2) The distance of each circuit breaker to the MCC is different, thus the latency in different routes is also different. Though the MCC sends out the reclose command every 0.1 s, the noncritical loads are not reconnected to the smart grid after each 0.1 s; 3) There is delay between the real dc bus voltage value and the dc bus voltage detected by the MCC, which causes the reopen time of the CB3 to be delayed. As a result, the dc bus voltage drops below the threshold voltage and causes a bigger ac bus voltage drop.

In conclusion, the communication network brings great benefits to the operation of the smart grid in allowing for implementation of new and different types of protection schemes and control. However, it is seen from Fig. 10(a) and (b) that without simulating the communication network, the actual system response cannot be accurately predicted. The real-time simulation platform presented in this paper integrates both the power system and the communication system, thus provides an effective method to study the communication system in smart grids.

VI. Conclusion

This paper presents the latest state-of-the-art technology on real-time simulation of smart grids. On one hand, compared to the real-time simulation of traditional power grid and simple power electronics circuit, the large numbers of high-speed switching devices in smart grids introduce significant challenges to the simulation. The real-time simulation platform presented in this paper utilizes switch event interpolation, SSN solver, and parallel computation technologies; combined with the advanced hardware platform, this system can achieve real-time simulation with hundreds of switches at switching frequencies up to 10 kHz. On the other hand, the characteristics of smart grids are greatly depending on the communication network. When combining the advanced power systems simulator with a state-of-the-art network simulator, this system can simulate the communication network in smart grids and provide great convenience for related study.

A microgrid model of a small community is built with the aforementioned technologies. The real-time model contains most of critical units in smart grids, including LES, PV, wind turbine, power conditioning circuits, solid state switches, and a comprehensive communication network. First, simulations were carried out without communication latency. It is verified that the system is capable of simulating detailed simulation models with a large group of switches at 10 kHz. Also, the proposed control strategies for seamless transition from grid-connected mode to islanding mode were verified. The simulation only utilizes no more than 10% of the calculation capability of the proposed platform.

Then, with the SITL technology provided by OPNET, a communication network is simulated together with the power network at real time. An external MCC is utilized as the system level controller with the help of the communication network, which can be easily adjusted based on different smart grid communication network structures. The distributed local control of inverters and converters is embedded in the model of each energy source and load. The simulation results show the effectiveness of the presented comprehensive simulation platform as well as the importance of an accurate and detailed simulation approach to evaluate the interactions between the communication and power networks in smart grids. As explained and demonstrated in the paper, the platform can be utilized to study difference scales of smart grid applications. New control strategies, such as dynamic reconfiguration of both communication and power network within a smart grid, could also be verified with this platform.

References

[1] R. Brown, "Impact of smart grid on distribution system design," in *Proc. IEEE Power Energy Soc. Gen. Meeting*, 2008, pp. 1–4.

[2] P. Parikh, M. Kanabar, and T. Sidhu, "Opportunities and challenges of wireless communication technologies for smart grid applications," in *Proc. CCECS Power Energy Soc. Gen. Meeting*, 2010, pp. 1–7.

[3] R. H. Lasseter, J. H. Eto, B. Schenkman, J. Stevens, H. Vollkommer, D. Klapp, E. Linton, H. Hurtado, and J. Roy, "CERTS Microgrid laboratory test bed," *IEEE Trans. Power Del.*, vol. 26, no. 1, pp. 325–332, Jan. 2011.

[4] M. Mao, M. Ding, J. Su, L. Chang, M. Sun, and G. Zhang, "Testbed for microgrid with multi-energy generators," in *Proc. IEEE Can. Conf. Elect. Comput. Eng.*, 2008, pp. 637–640.

[5] W. Li, G. Joos, and J. Belanger, "Real-time simulation of a wind turbine generator coupled with a battery supercapacitor energy storage system," *IEEE Trans. Ind. Electron.*, vol. 57, no. 4, pp. 1137–1145, Apr. 2010.

[6] D. Brandt, R. Wachal, R. Valiquette, and R. Wierckx, "Closed loop testing of a joint Var controller using a digital real-time simulator," *IEEE Trans. Power Syst.*, vol. 6, no. 3, pp. 1140–1146, Aug. 1991.

[7] S. Abourda, J. Belanger, and C. Dufour, "Real-time HIL simulation of a complete PMSM drive at 10 μs time step," in *Proc. IEEE Eur. Conf. Power Electron. Appl.*, 2005, pp. P-3–P-9.

[8] M. Matar and R. Iravani, "FPGA implementation of the power electronic converter model for real-time simulation of electromagnetic transients," *IEEE Trans. Power Del.*, vol. 25, no. 2, pp. 852–860, Apr. 2010.

[9] Y. Li, D. Vilathgamuwa, and P. Loh, "Design, analysis, and real-time testing of a controller for multibus microgrid system," *IEEE Trans. Power Electron.*, vol. 19, no. 5, pp. 1195–1204, Sep. 2004.

[10] J. Nutaro, P. Kuruganti, M. Shankar, L. Miller, and S. Mullen, "Integrated modeling of the electric grid, communications, and control," *Int. J. Energy Sector Manag.*, vol. 2, no. 3, pp. 420–438, 2008.

[11] M. Kezunovic, "Teaching the smart grid fundamentals using modeling, simulation, and hands-on laboratory experiments," in *Proc. IEEE Power Energy Soc. Gen. Meeting*, 2010, pp. 1–6.

[12] M. Brenna, E. De Berardinis, L. D. Carpini, P. Paulon, P. Petroni, G. Sapienza, G. Scrosati, and D. Zaninelli, "Real time simulation of smart grids for interface protection test and analysis," in *Proc. Int. Conf. Harmon. Quality Power*, 2010, pp. 1–6.

[13] R. Reddi and A. Srivastava, "Real time test bed development for power system operation, control and cyber security," in *Proc. North Amer. Power Symp.*, 2010, pp. 1–6.

[14] E. Felemban and E. Ekici, "Single Hop IEEE 802.11 DCF analysis revisited: Accurate modeling of channel access delay and throughput for saturated and unsaturated traffic cases," *IEEE Trans. Wireless Commun.*, vol. 10, no. 10, pp. 3256–3266, Oct. 2011.

[15] Opal-RT Technologies. [Online]. Available: http://www.opalrt.com

[16] Dolphin. [Online]. Available: http://www.dolphinics.com

[17] C. Dufour, J. Mahseredjian, and J. Belanger, "A combined state-space nodal method for the simulation of power system transients," *IEEE Trans. Power Del.*, vol. 26, no. 2, pp. 928–935, Apr. 2011.

[18] OPNET. [Online]. Available: http://www.opnet.com

[19] Y. Hu, B. J. Yurkovich, S. Yurkovich, and Y. Guezennec, "A technique for dynamic battery model identification in automotive applications using linear parameter varying structures," *IFAC Control Eng. Pract.*, vol. 17, no. 10, pp. 1190–1201, Oct. 2009.

[20] Y. Hu, B. J. Yurkovich, S. Yurkovich, and Y. Guezennec, "Electrothermal battery modeling and identification for automotive applications," *J. Power Sources*, vol. 196, no. 1, pp. 449–457, Jan. 2011.

[21] Y. Hu and S. Yurkovich, "Battery state of charge estimation in automotive applications using LPV techniques," in *Proc. ACC*, Baltimore, MD, USA, Jun. 2010, pp. 5043–5049.

[22] Y. Hu, B. J. Yurkovich, S. Yurkovich, Y. Guezennec, and R. Bornatico, "Model-based calibration for battery characterization in HEV applications," in *Proc. ACC*, Seattle, WA, USA, Jun. 2008, pp. 318–325.

[23] M. G. Villalva, J. R. Gazoli, and E. R. Filho, "Comprehensive approach to modeling and simulation of photovoltaic arrays," *IEEE Trans. Power Electron.*, vol. 24, no. 5, pp. 1198–1208, May 2009.

[24] H. J. Laaksonen, "Protection principles for future Microgrids," *IEEE Trans. Power Electron.*, vol. 25, no. 12, pp. 2910–2918, Dec. 2010.

[25] R. Pena, J. C. Clare, and G. M. Asher, "Doubly fed induction generator using back-to-back PWM converters and its application to variable-speed wind-energy generation," in *Proc. Inst. Elect. Eng.—Elect. Power Appl.*, 1996, pp. 231–241.

[26] S. Conti and S. Raiti, "Integrated protection scheme to coordinate MV distribution network DG interface protections and Micro-grid operation," in *Proc. IEEE Int. Conf. Clean Elect. Power*, 2009, pp. 640–646.

Feng Guo (S'09) was born in Henan, China, in 1986. He received the B.S. degree in electrical engineering from Wuhan University, Wuhan, China, in 2009. Currently, he is working toward the Ph.D. degree at The Ohio State University, Columbus, OH, USA.

His current research interests include large-scale photovoltaic power plants, hardware-in-the-loop, and real-time simulation of smart grids, power electronics circuits in hybrid electric vehicles, and energy harvesting around high-voltage transmission lines.

Luis Herrera (S'10) received the B.S. degree in electrical engineering from the University of Tennessee at Martin, TN, USA, in 2010. Currently, he is working toward the Ph.D. degree at The Ohio State University, Columbus, OH, USA.

His current research interests include modeling and networked control of the smart grid, hardware-in-the-loop, and field-programmable gate array modeling of fast switching power electronics, and high-frequency battery impedance testing.

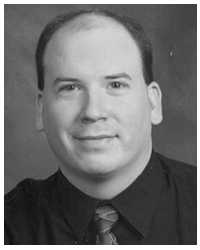

Robert Murawski (S'10–M'12) received the B.S. and M.S. degrees in electrical engineering from The Cleveland State University, Cleveland, OH, USA, in 2003 and 2004, respectively. He received the Ph.D. degree in electrical engineering from The Ohio State University, Columbus, OH, USA, in 2011.

Currently, he is working for QinetiQ North America at the NASA Glenn Research Center under the Space, Communication, and Navigation Program. His research interests include wireless networking, cognitive radio networks, and space-link communication emulation.

Ernesto Inoa (S'10) was born in the Dominican Republic. He received the B.S. degree in electronics engineering (*magna cum laude*) from the Pontificia Universidad Católica Madre y Maestra, Dominican Republic, in 2000, and the Master's degree in electrical and computer engineering from the University of Central Florida, Orlando, FL, USA, in 2005. He is currently working toward the Ph.D. degree at The Ohio State University, Columbus, OH, USA.

He worked as an Automation Engineer for Cerveceria Nacional Dominicana, a Dominican brewing company, where he helped automate several bottling lines with the use of programmable logic controllers. His major research interests are related to the application of novel control techniques to power electronics, motor drives, and energy conversion systems.

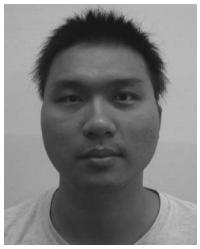

Chih-Lun Wang received the B.S. degree from National Chiao-Tung University, Hsinchu, Taiwan, in 2007 and the M.S. degree from The Ohio State University, Columbus, OH, USA, in 2010, both in electrical engineering.

His research interests include power system simulation and power electronic circuit design. In 2011, he joined Ford Motor Company, Dearborn, MI, USA, where he is currently a Power Electronic Engineer, working on power components characterization.

Philippe Beauchamp received the B.S. degree in software engineering with a specialization in control from the École Polytechnique de Montréal, Montréal, QC, Canada in 2006. He is currently working toward the M.B.A. degree at HEC Montreal.

He joined Opal-RT Technologies, Montreal, in 2006 as a Simulation Specialist in the integration team and held positions in R&D and technical sales. Currently, he is managing business development for the academic market in North America. His current fields of interest include real-time simulation and distributed computing applied to renewable energy, hardware-in-the-loop testing, and field-programmable gate array co-simulation.

Eylem Ekici (S'99–M'02–SM'11) received the B.S. and M.S. degrees in computer engineering from Bogazici University, Istanbul, Turkey, in 1997 and 1998, respectively. He received the Ph.D. degree in electrical and computer engineering from Georgia Institute of Technology, Atlanta, GA, USA, in 2002.

Currently, he is an Associate Professor in the Department of Electrical and Computer Engineering of The Ohio State University, Columbus, OH, USA. His current research interests include cognitive radio networks, vehicular communication systems, nanoscale networks, and wireless sensor networks, with a focus on routing and medium access control protocols, resource management, and analysis of network architectures and protocols. He is an Associate Editor of the IEEE/ACM TRANSACTIONS ON NETWORKING, *Computer Networks Journal* (Elsevier), and *ACM Mobile Computing and Communications Review*.

Jin Wang (S'02–M'05) received the B.S. degree from Xi'an Jiaotong University, Xi'an, China, in 1998, the M.S. degree from Wuhan University, Wuhan, China, in 2001, and the Ph.D. degree from Michigan State University, East Lansing, MI, USA, in 2005, all in electrical engineering.

From September 2005 to August 2007, he worked at the Ford Motor Company as a Core Power Electronics Engineer and contributed to the traction drive design of the Ford Fusion Hybrid. Since September 2007, he has been an Assistant Professor in the Department of Electrical and Computer Engineering, The Ohio State University, Columbus, OH, USA. His teaching position is co-sponsored by American Electric Power, Duke/Synergy, and FirstEnergy. His research interests include high-voltage and high-power converters/inverters, integration of renewable energy sources, and electrification of transportation.

Dr. Wang received the IEEE Power Electronics Society Richard M. Bass Young Engineer Award and the National Science Foundation's CAREER Award, both in 2011. He has over 50 peer-reviewed journal and conference publications. Dr. Wang has been an Associate Editor for the IEEE TRANSACTIONS ON INDUSTRY APPLICATIONS since March 2008.